Adakitic Volcanism in Sahand Region, Northwest Iran: Geochemical and Geodynamic Implications

Farhad Pirmohammadi Alishah[1*], Ahmad Jahangiri[2]

1- Department of Geology, Shabestar Branch, Islamic Azad University, Shabestar, Iran
2- Department of Geology, University of Tabriz, Tabriz, Iran

* Corresponding Author: Petrofarhad@yahoo.com

Received: 01 September 2013 / Accepted: 12 November 2013 / Published online: 17 November 2013

Abstract

We present new whole major and trace elements data for a suite of adakitic dacite to rhyolite rocks from the Sahand region. These rocks formed in the Pliocene to Pleistocene during the the collision between the Arabian and Eurasian plates following subduction of Neo–Tethys Ocean. These subvolcanic intrusions were emplaced into late Cretaceous and Eocene sedimentary، volcano–clastic and volcanic rocks. Geochemical data indicate that the subalkaline dacitic to rhyodacitic rocks have an adakitic characteristics with Na_2O/K_2O (1.8–3.16), high Sr (391–804ppm), Mg# = (18–57) and low Y (3.6–20.8 ppm), low Yb (0.65–1.29 ppm), and low heavy rare earth element (HREE) abundances. Fractionated REE patterns with, $(Ce/Yb)_N$ = 10–27, absence of negative Eu anomalies, low content of Y, Nb, Ti, and high Sr/Y ratios (74–265) suggest that the source was likely hydrous garnet–amphibolite or eclogite, possibly generated during subduction of the Neo–Tethyan oceanic slab beneath the Central Iran microplate. The adakitic volcanism was followed by eruption of alkaline magmatism in this area. Slab melting occurred after cessation of subduction, possibility cause by the collision. Transtensional tectonics accompanied by a locally extensional stress regime is account for magma genesis and ascent.

Keywords: Sahand, Post–collision, Dacite, Adakite, Neo–Tethys, Iran.

1–Introduction

The study areas are situated at Central Iran zone (Berberian and King, 1981) and are important parts of the collisional zone between the Arabian and Eurasia plates; (Mohajjel et al., 2003; Jahangiri, 2007) .Following the closure of Neo–Tethys and collision of the plates in the late Cretaceous, convergence continued and became more intense in the Pliocene (Jahangiri, 2007). This process caused considerable shortening, thickening and uplifting in NW Iran and East of Turkey (Pirmoahmmadi–Alishah, 2011). Meanwhile wide–spread Pliocene to Pleistocene volcanic activities occurred.

Alkaline rocks are also reported locally by Amidi (1984), Hassanzadeh (1993) and Moradian (1997). Amidi (1984) proposed a rift model to interpret the genesis of Eocene magmatic rocks in the UDMA. Berberian (1981) argued that the onset of alkaline volcanism, which followed the calc–alkaline volcanism (6–5 Ma) in UDMA was due to sinking of the final broken pieces of oceanic slab to a depth where alkaline melts were generated. Ghasemi (2006) suggested that post–suturing magmatic activity along the Sanandaj–Sirjan zone and UDMA can be attributed to slab break–off. In UDMA, the district of Sahand, and the Islamic Icland contain a geologic complexity and magmatic variation from calc–alkaline to alkaline is observed. The diversity of magmatic types from calk–alkaline to alkaline indicates that the region of Sahand, and the Islamic Icland represents young volcanic activity (Pirmoahmmadi–Alishah, 2011). The

most intense eruptions were occured during the post–collisional stage, which led to the formation of large volcanoes like Sahand, Sabalan and other volcanoes in this region. The great diversity of Neogene to Quaternary magmatic rocks, from andesitic, dacitic to rhyodacitic subvolcanic domes and their range for more than 150 km, are of interest due to their specific conditions of formation and their spatial and temporal relation with other magmatic rocks in this region. The dacitic volcanism in the late Pliocene and Pleistocene in this area was followed by alkaline volcanism (Jahangiri, 2007).

A conspicuous characteristic of this phase is the contemporaneous eruptions of mafic alkaline melts including melafoidites and alkali basalts (Berberian and King, 1981; Hassanzadeh, 1993). The temporal and spatial relationship of dacitic calc–alkaline magmatism with alkaline volcanism is also reported from different areas of Gondwana fragments and Eurasia plate collision zone (Pe–Piper et al., 1994; Seghedi et al., 2004; Chung et al., 2005).

The aims of this paper are (1) to present chemical characteristics of the dacitic to rhyodacitic magmatism in northwest Iran, (2) to interpret the conditions of their genesis, and (3) to discuss the geodynamic environment in which they could have formed.

2– Regional Setting

The Sahand volcanic body covers an area of 7200 km2 and reaches a maximum elevation of 3595 m above sea level. It is situated in northwest Iran, between the Tabriz and Maragheh cities. In the study area (Fig. 1), volcanic rocks consist of a wide range of pyroclastics, epiclastics and lavas, (Jahangiri, 2007) which can be seen in different forms, such as flow lavas, domes and stratovolcano units.

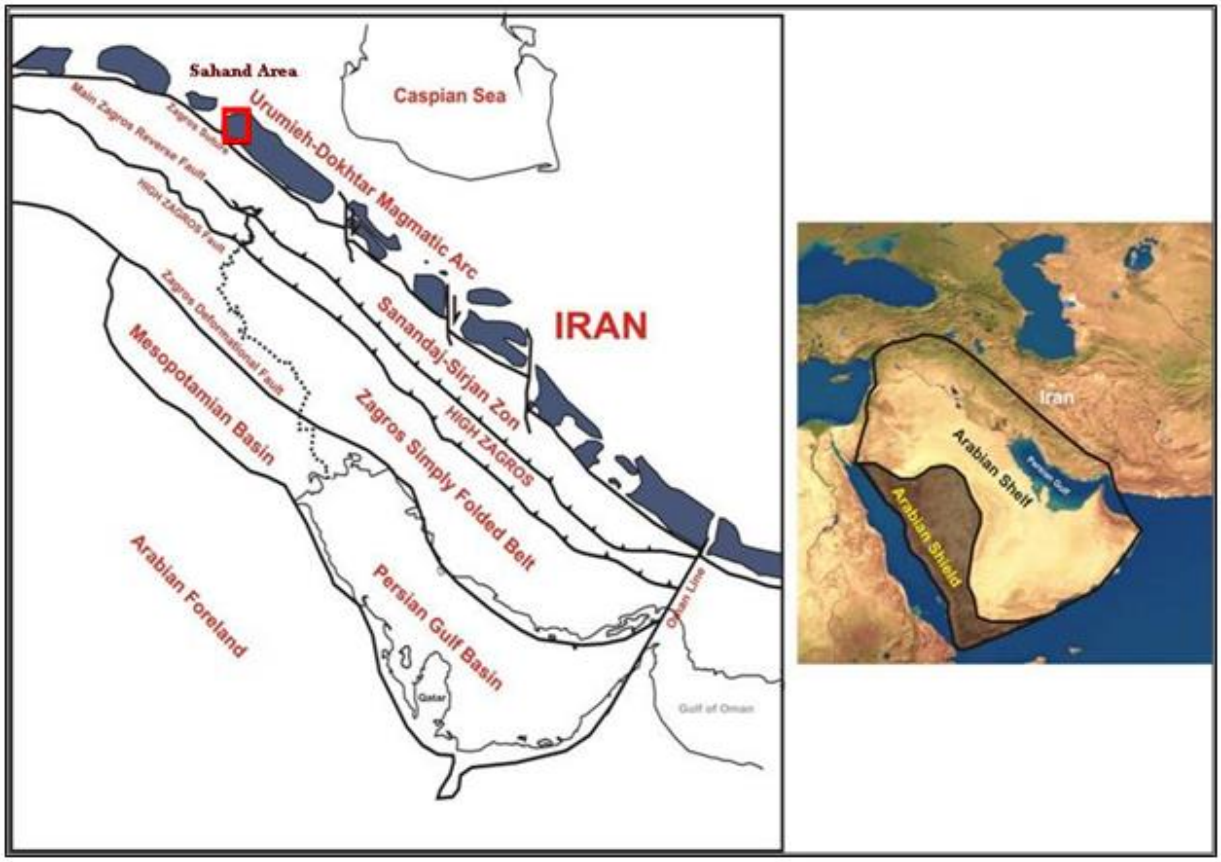

Figure 1) Three main tectonic units of the Zagros orogenic belt. The studied area is outlined by the box. Map from Allen et al. (2004).

These rocks have erupted with a distinct temporal pattern, so that pyroclastic rocks have considerable thickness and explosive facies are formed at the onset of each eruption, (Pirmoahmmadi–Alishah, 2011). Pyroclastic volcanic units cut the upper red formation sediments with upper Miocene age, or cover them with angular discontinuity in most of the studied areas (Pirmohammadi–Alishah, 2011). The investigated areas are situated at the Urumieh–Dokhtar Magmatic Arc (UDMA), south and southeast of Tabriz City (Fig. 1). These regions are situated between the Tabriz fault and the Urmieh Lake (Fig. 2). In this area, numerous (n~60) subvolcanic domes have intruded into the Eocene and Oligocen volcanics and the volcano–sedimentary rocks of UDMA (Fig. 3).

Field observations and the comparison of Figures 2 and 3, indicate that these andesitic and dacitic rocks were emplaced along faults and fractures. It is believed that the ascent of acidic magmas may have been related to the fault activity in this area (Fig. 3).

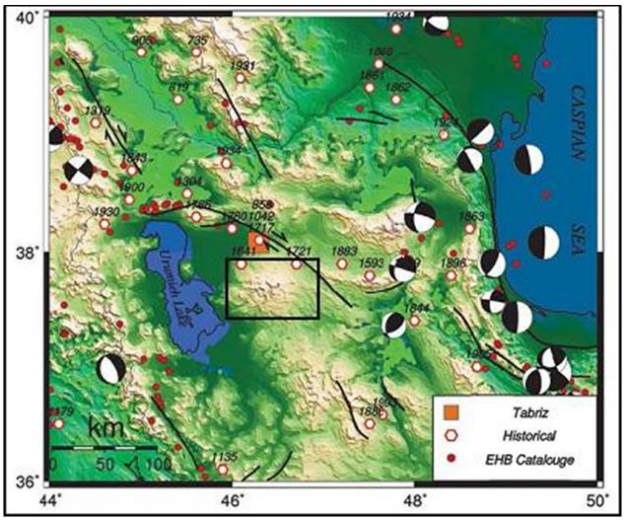

Figure 2) Tectonic map of the studied area that show by a square, studied area bounded by Tabriz fault and Urumieh Lake (Ambraseys and Melville., 1982).

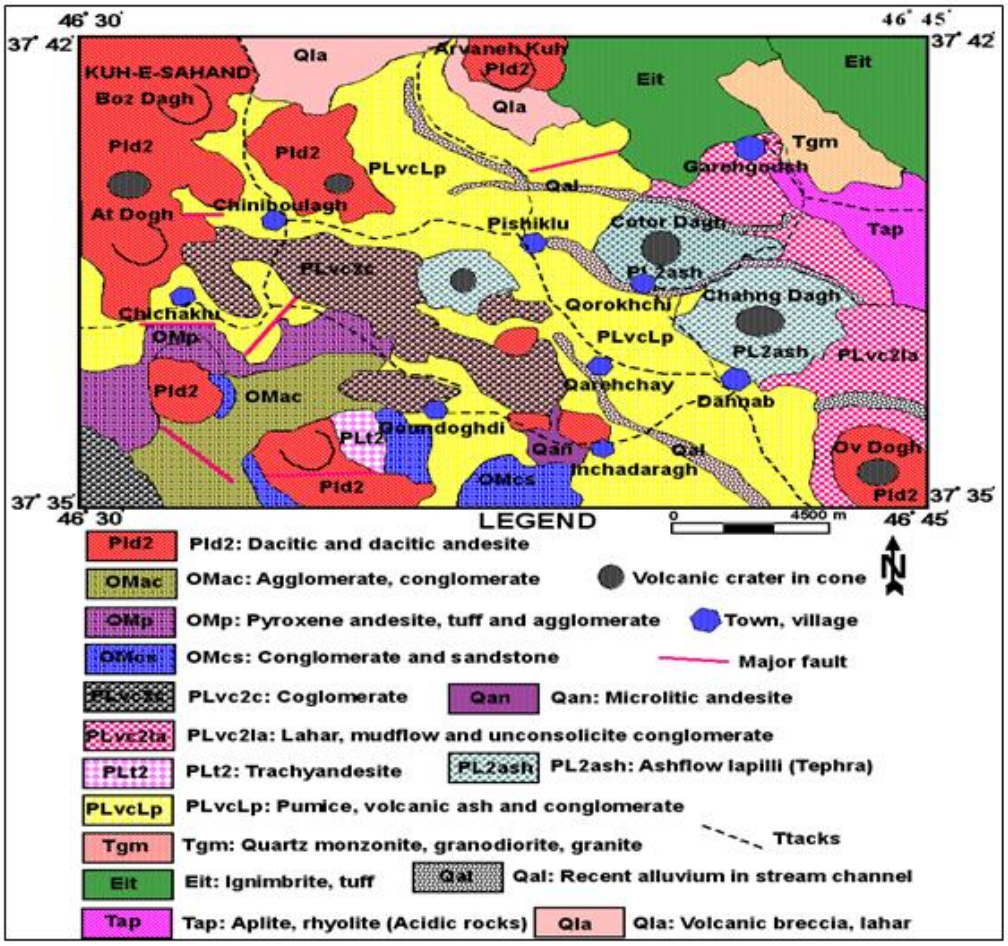

Figure 3) Geological map of the study area, adapted from the 1:100000 geological map of Bostanabad (Behrouzi et al., 1997).

The Eocene volcanic and volcaniclastic rocks consist of basalt, andesitic–basalt, brecciated volcaniclastic rocks and tuffs. The Oligocene dioritic plutons consist of porphyritic diorite, granodiorite and quartz–diorite rocks. The age of emplacement of subvolcanic domes has been determined by Moradian (1997), which yield ages 7–17 Ma based on K/Ar dating of amphibole and biotite.

3– Petrographic Features

The volcanic rocks in the study areas consist of andesite, dacite, rhyodacite, rhyolite and intermediate to acidic suites, with compositions varying from hornblende–andesite, dacite and rhyodacite. Dacitic and rhyodacite rocks are dominant and show porphyritic texture with phenocrysts of plagioclase, hornblende and biotite.

Table 1) Major and trace element contents of representative adakitic samples of Sahand.

sample	A7	B8	B9	C11	C16	C18	D21	E22	F27	F28	G1	G10	G11	H1
SiO_2 (Wt%)	69	69.4	67.9	66.2	58.2	67.6	67.2	68.2	67.1	67.1	67.6	67	65.8	67.4
Al_2O_3(Wt%)	15.65	15.9	15.75	16.25	17.5	16.25	16.25	16.05	16	15.1	15.65	16.65	15.8	15.95
Fe_2O_3(Wt%)	1.07	0.89	1.04	1.5	2.54	1.5	1.53	0.96	1.46	0.9	0.96	1.53	1.42	1.48
FeO(Wt%)	0.99	0.88	0.99	1.55	3.39	1.5	1.47	0.99	1.46	0.92	1	1.56	1.46	1.48
CaO(Wt%)	2.76	3.09	2.79	3.68	6.17	3.66	3.57	3.27	3.59	4.49	3.38	3.75	4.28	3.81
MgO(Wt%)	0.7	0.69	0.75	1.12	2.63	0.78	1.08	0.81	1.15	0.75	1.06	0.94	1.25	1.46
Na_2O(Wt%)	4.83	4.5	4.78	4.43	3.68	4.56	4.7	4.6	4.25	4.37	4.2	4.62	4.42	4.45
K_2O(Wt%)	2.27	2.16	2.3	2.06	1.96	2.15	2.34	1.78	2.52	2.32	2.35	2.32	2.26	2.22
Cr_2O_3(Wt%)	0.01	0.01	0.02	0.03	0.01	0.02	0.02	0.01	0.01	0.01	0.01	0.02	0.02	0.02
TiO_2(Wt%)	0.31	0.25	0.32	0.41	0.66	0.4	0.38	0.27	0.38	0.27	0.37	0.45	0.38	0.38
MnO(Wt%)	0.03	0.03	0.03	0.05	0.13	0.04	0.05	0.03	0.06	0.03	0.05	0.05	0.05	0.06
P_2O_5(Wt%)	0.13	0.09	0.13	0.18	0.23	0.19	0.19	0.1	0.18	0.1	0.14	0.22	0.18	0.13
SrO(Wt%)	0.06	0.06	0.06	0.06	0.05	0.07	0.08	0.06	0.06	0.06	0.05	0.07	0.07	0.07
BaO(Wt%)	0.07	0.08	0.07	0.08	0.06	0.08	0.09	0.06	0.07	0.08	0.07	0.1	0.09	0.08
LOI(Wt%)	1.7	2.09	2.7	1.89	1.89	0.5	0.8	2.3	1.8	3.3	2.17	0.79	2.5	1.09
Total(Wt%)	99.5	100	99.7	99.6	99.5	99.4	99.9	99.5	100	99.8	100	100	100	100
Ba (ppm)	607	672	622	619	530	689	762	538	617	654	608	839	713	704
Ce (ppm)	54.7	38.6	54.4	52.2	50.1	52.3	52.1	32.7	47.7	40.9	45.2	53.3	50.4	47.3
Co (ppm)	4.1	3.9	4.8	7.5	16.7	6.2	7.8	4.5	6.9	4.1	6.4	6.8	6.9	8.3
Cr (ppm)	70	90	130	200	90	150	100	90	90	60	90	130	110	110
Cs (ppm)	1.15	1.64	1.13	1.34	2.42	1.67	1.67	1.28	2.18	1.87	2.41	1.2	2.45	2.81
Cu (ppm)	11	39	11	20	45	25	22	11	12	17	19	32	29	25
Dy (ppm)	1.08	0.9	1.04	1.79	3.84	1.57	1.54	0.9	1.55	0.95	1.6	1.59	1.39	1.52
Er (ppm)	0.5	0.43	0.48	0.92	2.39	0.81	0.85	0.45	0.83	0.48	0.81	0.78	0.7	0.75
Eu (ppm)	0.67	0.61	0.66	0.93	1.13	0.84	0.88	0.56	0.8	0.65	0.76	0.89	0.8	0.77
Ga (ppm)	18.4	17.5	18.7	19.1	18.3	19	18.9	17.2	18.4	17.6	18	19.5	18.1	18.9
Gd (ppm)	2.38	1.93	2.35	3.05	4.53	2.85	2.71	1.63	2.6	1.96	2.54	2.76	2.6	2.89
Hf (ppm)	4	3.2	4	4.2	4.2	3.6	3.4	3	3.5	3.2	3.5	4	3.5	3.3
Ho (ppm)	0.18	0.16	0.18	0.32	0.79	0.29	0.29	0.16	0.28	0.17	0.29	0.29	0.24	0.27
La (ppm)	36	25.4	35.6	30	26.5	31.7	29.7	21.3	27.5	25.3	27.1	31.7	29.2	27.3
Lu (ppm)	0.05	0.05	0.05	0.12	0.36	0.09	0.11	0.05	0.11	0.06	0.1	0.1	0.08	0.08
Mo(ppm)	4	4	4	4	5	3	3	2	3	3	3	5	5	3
Nb (ppm)	12.5	8.1	12.6	10.6	10.4	10.4	12.8	7.5	11.2	9	10	12.7	9.9	10.7
Nd (ppm)	17	13.2	16.6	20	22.4	19.6	19.2	10.7	17.6	13.3	16.6	19.5	18.2	17.8
Ni (ppm)	8	17	14	15	9	13	8	11	9	6	7	12	11	20
Pb (ppm)	14	16	15	14	12	15	17	13	16	15	16	17	15	19
Pr (ppm)	5.36	3.92	5.23	5.64	5.93	5.74	5.62	3.2	5.09	4.13	4.88	5.6	5.29	5.04
Rb (ppm)	47.7	51.3	45.9	42.9	83.1	46.9	52.7	43.6	52	54.1	55.2	48	48	54.9
Sm (ppm)	2.39	2	2.37	3.28	4.23	3.13	3.25	1.67	2.78	2.2	2.77	2.96	2.81	2.85
Sr (ppm)	444	513	438	433	391	533	652	476	508	463	424	580	561	550
Ta (ppm)	0.9	0.6	0.9	0.7	0.7	0.7	0.8	0.5	0.7	0.7	0.7	0.8	0.7	0.8
Tb (ppm)	0.25	0.21	0.25	0.38	0.68	0.33	0.33	0.2	0.31	0.23	0.32	0.34	0.3	0.31
Th (ppm)	13.5	9.26	13.4	8.35	11.3	7.75	8.2	8.3	7.85	9.16	8.44	8.61	7.22	7.56
Ti (ppm)	1858	1499	1918	2458	3956	2398	2278	1618	2278	1618	2218	2697	2278	2278
Tm (ppm)	0.07	0.07	0.08	0.12	0.34	0.1	0.1	0.06	0.12	0.06	0.1	0.11	0.09	0.11
U (ppm)	3.11	2.51	3.17	2.07	3.32	2.52	2.98	2.31	2.84	3.41	2.93	2.6	2.54	3
V (ppm)	28	23	27	48	133	51	36	27	52	26	50	61	53	57
W (ppm)	3	4	10	13	5	14	3	6	7	3	7	5	4	8
Y (ppm)	4.7	4.2	4.7	8.2	20.8	7.7	7.8	4.5	8	4.5	7.8	7.4	6.3	7.3
Yb (ppm)	0.39	0.34	0.4	0.74	2.27	0.65	0.72	0.39	0.71	0.43	0.67	0.71	0.61	0.71
Zn (ppm)	48	38	48	56	75	58	54	41	58	41	51	60	54	53
Zr (ppm)	161	121	158	160	147	139	137	112	132	121	134	154	127	119

Table 1) continued

sample	S1	No	N6	N4	N3	N2	N1	M3	M1	L6	L3	k2	J1	I5	I4	H3
SiO_2 (Wt%)	65.7	69.3	69.4	69.7	67.7	67.5	67.4	65.4	62.3	66.6	65.5	65.2	67.8	66.1	69.4	69.7
Al_2O_3(Wt%)	15.8	15.7	15.45	15.05	15.85	15.9	16.2	15.8	18.2	16.45	16.75	16.6	15.4	16.15	15.8	15.35
Fe_2O_3(Wt%)	1.41	1.7	1.68	0.91	1.38	1.47	1.48	1.58	1.12	1.81	1.88	1.71	0.98	1.5	0.92	1.64
FeO(Wt%)	1.51	0	0	0.88	1.43	1.5	1.48	1.62	1.37	1.75	2.03	1.83	1	1.57	0.87	0
CaO(Wt%)	3.81	3.43	2.99	2.97	3.58	3.63	3.64	3.7	1.76	3.49	4.05	4.26	3.15	3.75	3.04	3.02
MgO(Wt%)	1.39	0.71	0.72	0.73	1.17	1.18	0.84	1.28	0.16	0.52	0.76	0.88	0.81	1.34	0.74	0.79
Na_2O(Wt%)	4.33	4.88	4.76	4.62	4.47	4.4	4.58	4.44	3.11	4.66	4.23	4.28	4.63	4.11	4.8	4.29
K_2O(Wt%)	2.24	1.87	1.88	1.91	2.16	2.25	2.27	2.51	2.49	2.6	2.01	1.99	1.78	2.4	2.06	2.14
Cr_2O_3(Wt%)	0.02	0.01	0.01	0.02	0.02	0.02	0.01	0.02	0.01	0.02	0.01	0.01	0.02	0.01	0.02	0.01
TiO_2(Wt%)	0.37	0.22	0.22	0.22	0.37	0.37	0.4	0.39	0.45	0.42	0.46	0.45	0.26	0.42	0.23	0.21
MnO(Wt%)	0.05	0.03	0.03	0.03	0.05	0.05	0.05	0.06	0.02	0.03	0.03	0.04	0.03	0.05	0.03	0.03
P_2O_5(Wt%)	0.19	0.07	0.08	0.09	0.16	0.15	0.16	0.27	0.27	0.24	0.23	0.23	0.08	0.18	0.07	0.04
SrO(Wt%)	0.07	0.06	0.06	0.05	0.07	0.07	0.07	0.09	0.1	0.09	0.07	0.07	0.06	0.07	0.06	0.05
BaO(Wt%)	0.08	0.07	0.07	0.07	0.08	0.08	0.08	0.11	0.11	0.12	0.1	0.09	0.06	0.08	0.06	0.06
LOI(Wt%)	1.9	0.99	2	2.49	1.6	1.5	0.5	2.18	8.35	1	1.69	1.39	2.3	2.28	1.38	2.78
Total(Wt%)	99	99	99.4	99.8	100	100	99.3	99.6	99.9	100	100	99.2	98.4	100	99.5	100
Ba (ppm)	701	568	567	567	673	672	709	890	942	1025	856	776	509	699	521	523
Ce (ppm)	46.7	28.5	28.2	27.7	48.9	49.1	50.2	68.9	67.4	76.3	56.3	54.7	33.6	51.7	31.4	30.6
Co (ppm)	7.9	3.7	3.7	3.8	6.9	7.1	7.1	7	3.6	6.1	6.4	7.3	4.8	7.8	4.1	3.8
Cr (ppm)	120	90	80	110	100	140	70	120	70	110	70	100	130	100	110	70
Cs (ppm)	2.72	1.93	1.75	1.81	2.3	2.35	1.17	9.95	13.55	3.11	21.2	4.17	1.32	2.85	2.1	2.93
Cu (ppm)	31	15	27	15	25	24	44	29	22	32	43	41	21	20	10	10
Dy (ppm)	1.48	0.9	0.94	0.86	1.47	1.53	1.44	1.74	0.86	2.19	1.92	1.91	0.95	1.62	0.97	1
Er (ppm)	0.73	0.44	0.44	0.44	0.74	0.75	0.76	0.88	0.44	1.08	0.97	0.96	0.45	0.82	0.54	0.59
Eu (ppm)	0.77	0.48	0.47	0.45	0.75	0.76	0.75	1	0.61	1.16	1.02	1.05	0.55	0.83	0.53	0.52
Ga (ppm)	18.3	17	16.6	16.2	18.6	18.6	19	19.5	26.4	20	19	19.4	17.1	19.1	17.3	15.8
Gd (ppm)	2.62	1.48	1.55	1.49	2.49	2.51	2.64	3.4	2.18	3.97	3.42	3.58	1.72	2.83	1.74	1.74
Hf (ppm)	3.3	2.7	2.7	2.6	3.4	3.5	3.5	3.6	3.3	3.9	3.4	3.4	2.9	3.7	2.9	2.8
Ho (ppm)	0.26	0.16	0.16	0.14	0.26	0.27	0.25	0.3	0.13	0.37	0.33	0.35	0.17	0.28	0.19	0.19
La (ppm)	26.4	18.2	17.9	17.4	28.5	28.7	29.1	38.5	37.8	47	33.1	35.6	21.3	29.7	20.3	19.2
Lu (ppm)	0.09	0.05	0.05	0.05	0.1	0.1	0.09	0.11	0.04	0.13	0.1	0.1	0.05	0.11	0.07	0.08
Mo(ppm)	5	2	2	4	3	6	2	5	2	2	2	2	5	3	3	3
Nb (ppm)	10.7	7.5	7.2	7.3	10.2	10.3	10.8	16.1	11.7	15.5	12	12.5	7.5	11.9	8.7	8.1
Nd (ppm)	17.3	9.5	9.2	9.1	17.2	17.2	18	25.6	21.2	29.3	22	23.6	11.3	18.7	10.2	10
Ni (ppm)	16	8	9	8	9	10	12	12	7	16	11	13	12	13	8	8
Pb (ppm)	17	13	14	14	16	17	20	19	10	24	16	16	13	16	15	13
Pr (ppm)	4.99	2.79	2.77	2.76	5.16	5.19	5.37	7.5	7.2	8.67	6.23	6.66	3.4	5.44	3.12	3.03
Rb (ppm)	55.6	48.5	48.8	49.1	53.1	54.1	51.8	58.7	50.6	54.1	49.4	49.9	45.1	53.9	55.7	54
Sm (ppm)	2.83	1.48	1.44	1.46	2.67	2.63	2.79	3.72	2.26	4.34	3.57	3.82	1.77	2.93	1.67	1.65
Sr (ppm)	554	472	454	435	542	545	569	751	804	768	570	614	454	522	436	429
Ta (ppm)	0.8	0.6	0.6	0.6	0.7	0.7	0.7	0.1	0.8	1	0.8	0.8	0.5	0.8	0.7	0.6
Tb (ppm)	0.3	0.17	0.18	0.18	0.31	0.3	0.31	0.39	0.18	0.47	0.4	0.41	0.2	0.34	0.2	0.21
Th (ppm)	7.46	7.1	7.15	7.12	8.25	8.29	8.45	8.83	8.48	8.72	4.64	7.86	8.24	7.93	8.25	8.92
Ti (ppm)	221	1319	1319	1319	2218	2218	2398	2338	2697	2418	2757	2697	1558	2518	1379	1259
Tm (ppm)	0.09	0.06	0.06	0.05	0.1	0.1	0.09	0.11	0.02	0.14	0.12	0.12	0.06	0.1	0.06	0.08
U (ppm)	3.16	2.59	2.63	2.64	2.81	2.85	2.85	4.1	2.63	3.53	2.69	2.79	2.48	2.82	3.5	2.82
V (ppm)	54	21	22	24	54	57	53	52	59	50	71	73	29	57	22	24
W (ppm)	6	7	6	4	14	6	3	6	4	9	3	7	6	7	8	5
Y (ppm)	7	4.4	4.2	4.3	6.7	7.2	6.8	8.3	3.6	10.4	8.5	9.4	4.4	7.6	5.1	5.2
Yb (ppm)	0.66	0.37	0.39	0.37	0.64	0.62	0.67	0.74	0.32	0.88	0.78	0.73	0.38	0.71	0.49	0.53
Zn (ppm)	51	33	34	36	55	57	52	62	23	65	68	65	39	54	36	36
Zr (ppm)	124	100	102	98	127	129	130	134	119	154	125	129	110	143	110	100

Plagioclase is a ubiquitous phenocryst (25–50 vol. %) and contains inclusions of magnetite, amphibole and opaque. Andesites and dacites contain large plagioclase crystals (3–5 mm) that usually exhibit sieve textures and well defined zoning marked by concentric zones, which are commonly rich in glass and or opaque inclusions. In some samples, plagioclase phenocrysts are mantled by a rim devoid of inclusions, whereas the cores are rich in inclusions. Hornblende occurs as the main ferromagnesian phenocryst (up to 2 mm in size) in andesite and dacite and varies from green to brown in color. Hornblende is often opassitezied and altered to opaque iron oxides. In some samples, accumulation of hornblende led to the formation of glomeroporphyric texture. The groundmass is composed of plagioclase and hornblende as the main minerals, with apatite, biotite, quartz and iron oxides as accessory minerals. Heterogeneous mineralogy, field and textural evidences, such as sieve texture in plagioclase, high normative quartz and the resorbed rims of some of the minerals, e.g. amphibole and oscillatory zoning in plagioclase, all suggest that the primary magmas underwent a magmatic evolution including fractional

crystallization, crustal contamination and possibly magma mixing during their ascent.

4– Geochemical Characteristics

4.1– Analytical Method

In order to correctly characterize their chemical composition, 30 samples were chosen for major, trace and rare–earth element (REE) analysis. Samples for whole rock analysis were crushed and powdered in agate ball–mills. Major elements were determined by ME–ICP method. Inductively Coupled Plasma–Mass Spectrometry (ICP–MS) was employed for REE and trace element analysis for all of the samples. All of the analyses were determined at Actlabs Laboratories (Canada). Representative chemical analysis for major, trace and rare earth elements are presented in Table 1.

4.2– Analytical Results

This petrogenetic family, termed "adakites", was described by Defant and Drummond (1990) as high–alumina, intermediate to felsic volcanic rocks typically hosting phenocrysts of plagioclase, amphibole, mica and (rarely) orthopyroxene, and lacking phenocrysts of clinopyroxene. Accessory phases of titanomagnetite, apatite, zircon and titanite were identified as common but not ubiquitous. A complementary and broadly accepted chemical definition of adakites was subsequently provided by Defant and Kepezhinskas (2001): adakites are high–silica (SiO_2>56%), high–alumina (Al_2O_3>15%), plagioclase and amphibole–bearing lavas with Na_2O>3.5%, high Sr (>400ppm), low Y (<18ppm), high Sr/Y (>40), low Yb (<1.9), and high La/Yb>20. The SiO_2 of samples vary from 58.2 to 69.7 wt%. Using the SiO_2 vs. Zr/TiO_2 diagram of Winchester et al. (1977) for classification of volcanic rocks, the studied samples plot in the fields of andesite and dacite–rhyodacite (Fig. 4). These rocks are peraluminous with Al_2O_3/ ($CaO+Na_2O+K_2O$) ratios of 1.5–2.0.

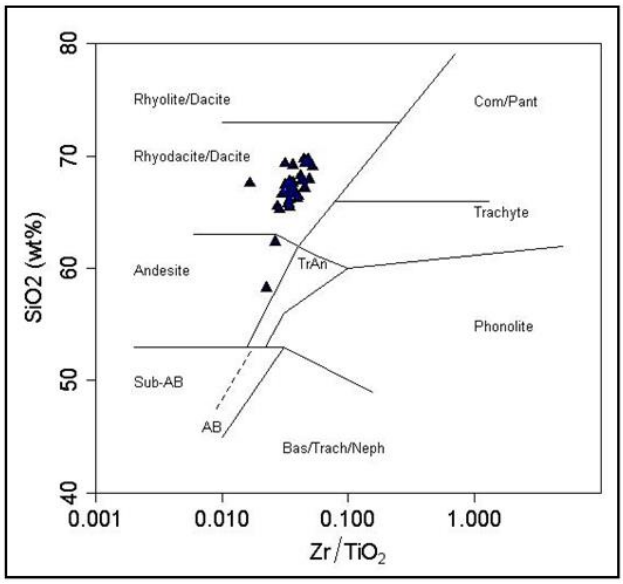

Figure 4) Classification of volcanic rocks by Zr/TiO_2 vs. SiO_2 (Winchester and Floyd., 1977). Sample compositions range from andesite, to dacite–rhyodacitic.

When applying SiO_2 as a fractionation index, the samples display chemical variation and crystal fractionation trends on Harker diagrams (Fig. 5).

The variation diagrams of Fe_2O_3, MgO, TiO_2 and CaO display negative correlations, suggesting that these volcanic rocks experienced fractionation of apatite, hornblende and plagioclase. The scatter of the samples is likely due to the presence of phenocrysts (fractional crystallization) or variable assimilation of continental crust. The other oxides and incompatible trace elements (e.g. K_2O, Na_2O, Zr, Ba and etc.) display more scattered trends. The K_2O/Na_2O ratios vary from 0.32 to 0.63 and samples are plot in the medium–potassium field and high potassium field (Fig. 6).

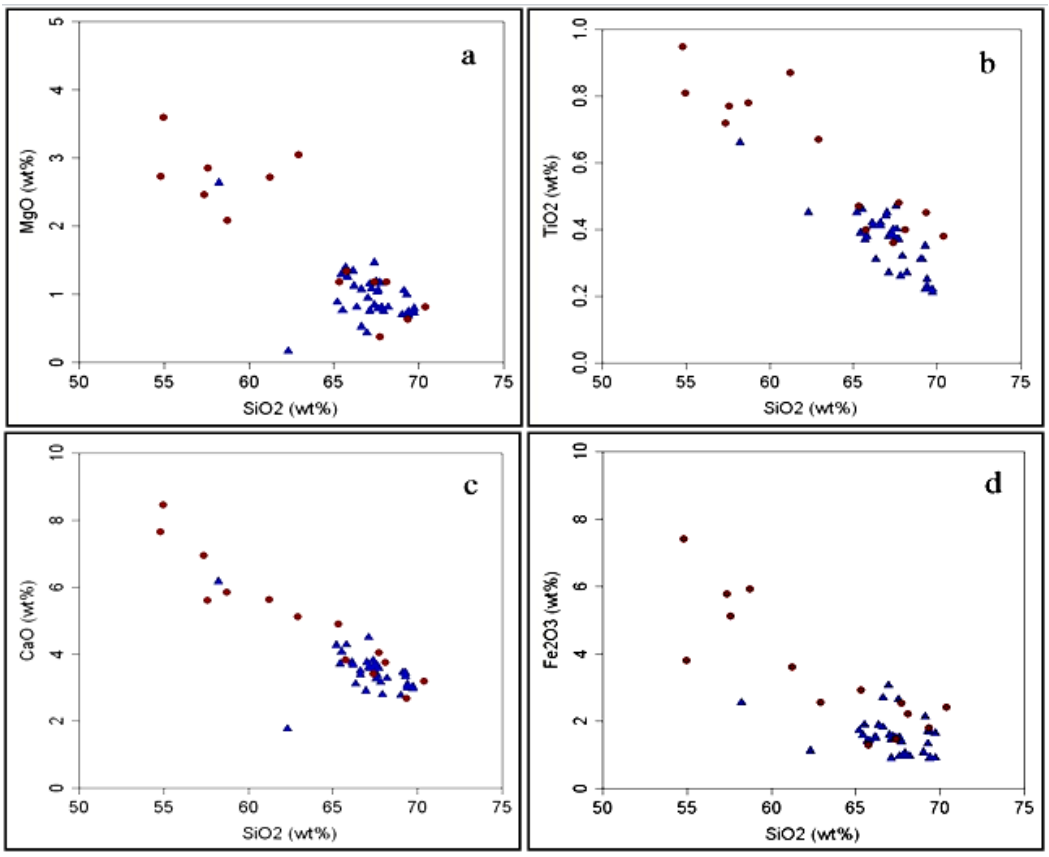

Figure 5) Variation diagrams for major elements (Harker 1909), ▲ Andesite, ● Dacite.

In the Na_2O+K_2O vs. SiO_2 diagram of Irvin and Baragar (1971), all of the samples plot in the subalkaline field (Fig. 7). The AFM diagram of (Irvin and Baragar, 1971, Fig. 8) displays a calk–alkaline serie. In the Y vs. Zr diagram (Maclean and Barrett, 1993) the sample plot in the calc–alkaline field (Fig. 9). The Mg # [MgO/(MgO+FeO)] of the samples ranges from 0.18 to 0.57 and they contain high concentration of Sr (584 to 1750 ppm) and low contents of Y and Rb. The high contents of Sr, low ratios of K_2O/Na_2O, Mg # (mean of 0.42) and high concentrations of Rb and Y indicate geochemical characteristics different from typical calc–alkaline volcanic rocks.

In the Y vs. Sr/Y diagram, all of the samples plot in the adakites field defined by (Defant and Drummond, 1990, Fig. 10). In the various trace and major elemental correlation diagrams the chemical compositions of the Sahand samples plot in the field of high–Si adakites (Martin et al., 2005, Fig. 11).

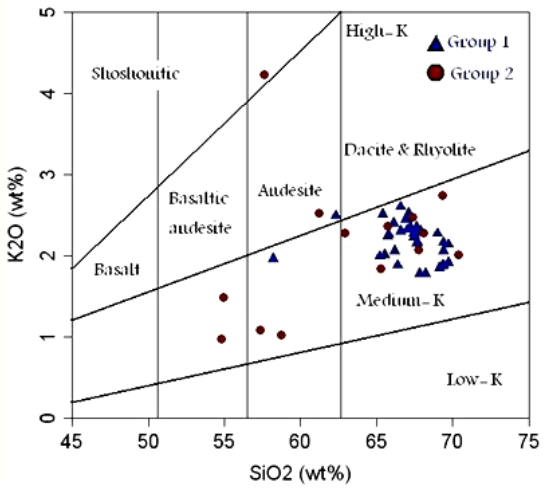

Figure 6) K_2O vs. SiO_2 for dacitic rocks of Central Volcanic Belt of Iran. Most of the samples plat in medium–k field and high–K (Gill, 1981), ▲ Andesite, ● Dacite.

Figure 12 shows a trace element diagram for representative samples from different domes normalized to primitive mantle composition (Sun and McDonough, 1989). All of the samples exhibit typical

subduction–related signatures, e.g. they are enriched in large ion lithophile elements (LILE), such as K, Rb and Ba and LREE relative to HFSE and HREE and they have negative Nb anomalies. They show significant positive anomalies for Sr, indicative of accumulation of plagioclase phenocrysts.

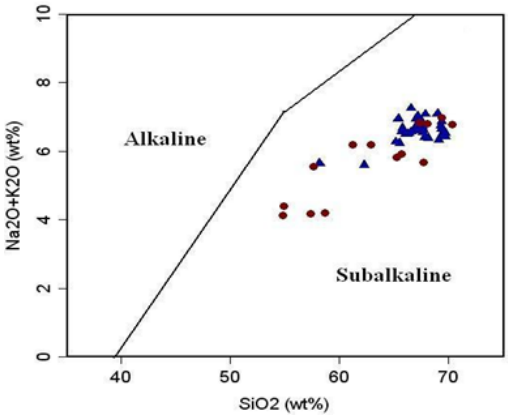

Figure 7) $Na_2O + K_2O$ vs. SiO_2 diagram (Irvin and Baragar, 1971), all of the samples plot in subalkaline field, ▲ Andesite, ● Dacite.

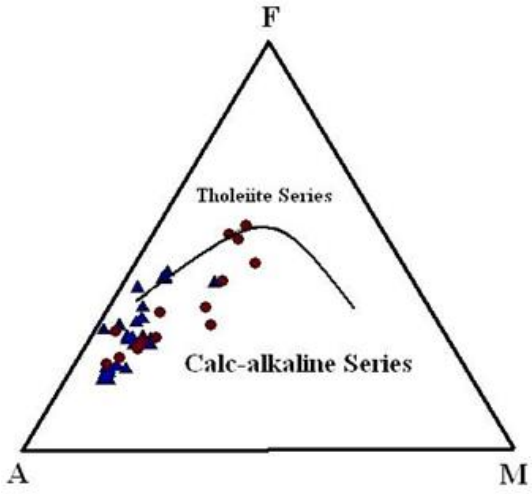

Figure 8. AFM diagram of (Irvin and Baragar., 1971). Most of the samples plot in Calc–Alkaline field, ▲ Andesite, ● Dacite.

The REE patterns for adakitic rocks from the study area are similar, although the abundances are variable. All the samples are enriched in LREE and strongly fractionated in LREE and have a flat MREE to HREE pattern (La_N/Yb_N values of 11 to 38).

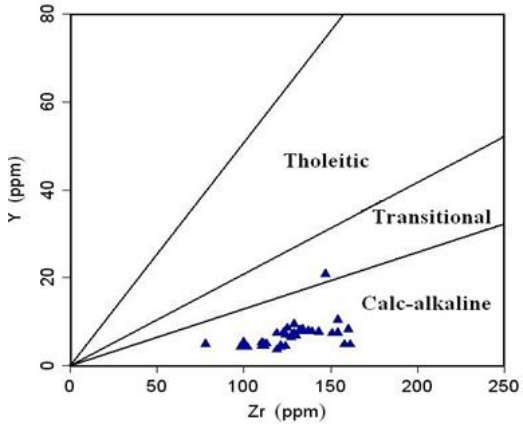

Figure 9) Diagram of Zr vs.Y after (Le–Maitre et al., 1989) all samples plot in the calc–alkaline field.

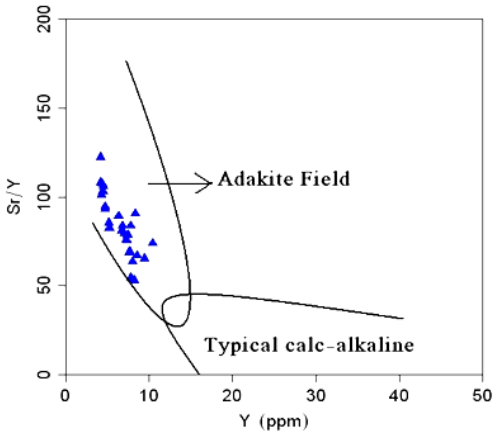

Figure 10) Sr/Y vs. Y diagram (Defant and Drummond, 1990) discriminating between adakitic and classical arc calc–alkaline compositions.

Figure 13 displays the incompatible trace elements patterns of representative samples normalized to the average N–MORB of Sun and McDonough (1989). Decoupling of Zr and Ti with similar bulk partition coefficients (Kd's), as seen by the greater depletion of Ti has been interpreted to reflect a residual phase in the source that fractionated Ti (Pearce and Parkinson, 1993) or Ti–bearing phases (Reagan and Gill, 1989). The strong depletion of Y and Yb corresponds to presence of a garnet–bearing restite in an eclogitic or garnet–amphibolite source. The REE concentrations for samples of the adakitic rocks from the study area are plotted

relative to chondrite in Figure 14. The ΣREE ranges from 61 to 173 ppm.

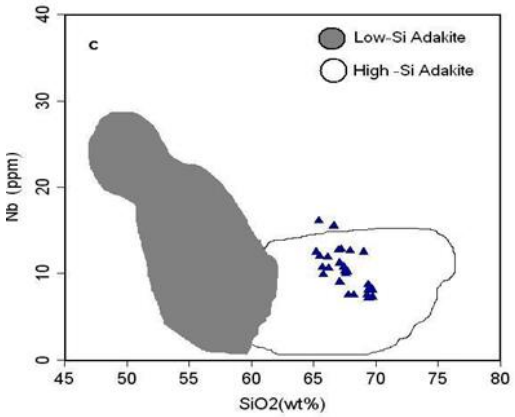

Figure 11) SiO_2 vs. Nb diagram (Martin et al., 2005) Sahand samples are plotted in the field of the high–Si adakite.

The REE patterns for the rocks from the study area are parallel with small positive Eu anomalies, implying their cogenetic nature and derivation from source regions that had homogeneous concentrations of REE and mineralogy. The parallel nature of the HREE patterns suggest that the residues had large partition coefficients for these elements, and consequently that they were likely garnet–rich.

5– Discussion

The degree to which anatexis of subducted oceanic crust has contributed to magmatism at convergent plate margins has been a point of controversy for decades (Derek et al., 2004). As discussed by Gill (1981), arc magmas of basaltic composition are regarded as products of mantle, not slab anatexis, although some later workers continued to suggest a role of slab anatexis in the production of arc basalts, particularly those with high Al–contents (Martin, 1999). Hydrated mantle peridotite as the principal source for arc basalts is now firmly established (Tatsumi and Koyaguchi, 1989), but genesis of intermediate and felsic arc magmas remains controversial. The issue of slab anatexis as a globally important process was emphasized by Defant and Drummond (1990) and Drummond and Defant (1990) who demonstrated a connection between subduction of young oceanic crust and production of intermediate to felsic igneous rocks, which bear the signature of a garnetiferous residuum.

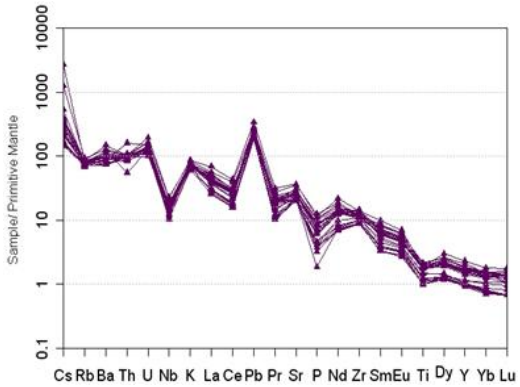

Figure 12. Primitive mantle–normalized incompatible trace element diagram for all samples (Sun and McDonough., 1989).

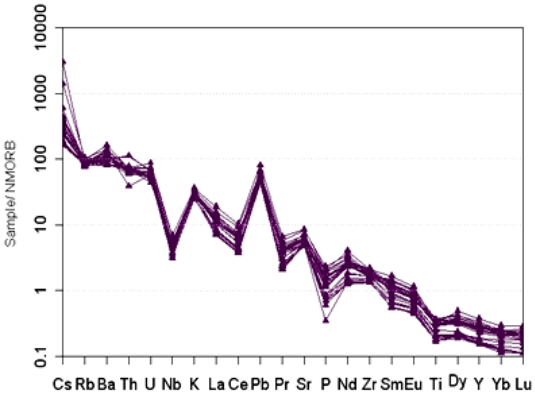

Figure 13) NORB–normalized incompatible trace element diagram for all samples (Sun and McDonough, 1989).

Such magmatic rocks are compositionally similar to Tertiary lavas on Adak Island in the Aleutian arc, which were identified as products of slab melting by Kay (1978). Geochemically, it appears that subduction related components played a critical role in the genesis of the dacitic magmas in Urumieh–Dokhtar Magmatic Arc (UDMA). Enrichment of LILE and depletion of HFSE (Nb and Ti) and HREE

are characteristic of subduction zone magmatism (Defant and Drummond, 1990; Defant and Kepezhinskas, 2001; Martin, 1999; Martin et al., 2004; Wilson, 1989). On the other hand the high ratios of Na_2O/K_2O, high Sr, Mg #, Sr/Y and $(Ce/Yb)_N$ suggest an adakitic character for subduction–related magmatism (Tatsumi and Koyaguchi, 1989; Defant and Drummond, 1990; Defant and Kepezhinskas, 2001; Martin et al., 2004).

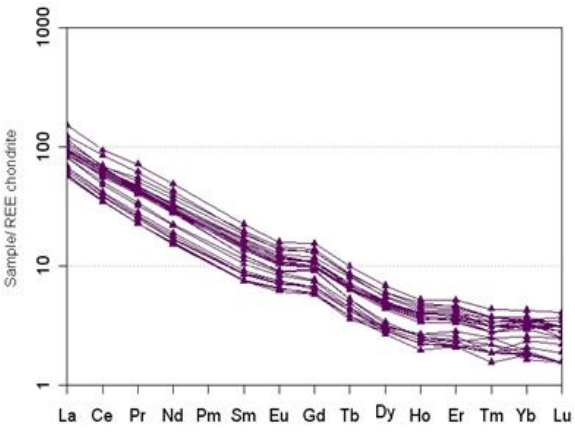

Figure 14) Chondrite–normalized REE pattern of representative dacitic samples of Central Iranian Volcanic Belt (Sun and McDonough, 1989).

The origin of adakites has been attributed to partial melting of either subducted oceanic crust converted to eclogite and garnet–amphibolites (Defant and Drummond., 1990; Drummond and Defant, 1990; Kay, 1978; Martin, 1993; Martin, 1999), or to underplating of basaltic magmas under thick continental crust (Atherton and Petford, 1993). The strongly fractionated REE pattern and depletions HREE and Y in adakites are possibly due to the presence of garnet +/− amphibole in melt residue. Their high Sr and low Nb, Ta, and Ti contents are thought to be due to absence of plagioclase and presence of Fe–Ti oxides in the residue (Martin, 1999). While geochemical data for igneous rocks compiled by Defant and Drummond (1990) indicate a relationship between subducted oceanic crust and adakite genesis, adakite occurrences in different tectonic environment led (Maury et al., 1996) to propose that slab melting even of old oceanic crust is also possible during: 1) the initiation of subduction (Sajona et al., 1993; Sajona et al., 1994), 2) fast and oblique subduction (Kay, 1978; Peacock et al., 1994) or 3) termination of subduction (Prouteau et al., 1996; Sajona, 2000). The high Mg and Cr content of most adakites are not consistent with the low concentration of these elements in experimentally produced melts of amphibolite or eclogite (Rapp et al., 1991; Sen and Dunn, 1995). Sen and Dunn (1994) and Yogodzinski et al. (1995) attributed this enrichment to the interaction of adakitic magma with the mantle wedge during ascent. Experimental work by Rapp et al. (1999) show that small amounts of adakitic melt are entirely consumed in reaction with mantle peridotite to from metasomatised zones as has been proposed by Seking and Wyllie (1982) and Sen and Dunn (1995). On the other hand, when the ratio of melt/peridotite reaches 2:1, a portion of melt not consumed in the reaction becomes Mg–enriched and preserves its trace element geochemical characteristics, such as high Sr/Y and $(Ce/Yb)_N$ ratios.

The highly enriched N–MORB normalized trace element patterns for adakitic dacitic and rhyodacites of UDMA (Sahand region), suggest the existence of garnet as a residue in the source. The enrichment of Sr and the absence of negative Eu anomalies indicate that the residual source was plagioclase–free. The Nb and Ti are strongly depleted in the studied samples, which suggest that the source also has residual rutile and amphibole and thus was

most probably hydrous garnet–amphibolite or eclogite. This garnet–bearing source implies that there are at least two possibilities for generation of adakitic rocks in Sahand: 1) partial melting of thickened lower crust and 2) melting of subducted oceanic slab of the Neotethys. It is expected that crustal thickening caused by the Arabian–Asian continental collision would result in transformation of basaltic lower crust in to garnet–amphibolite or eclogite. However, such deeper crustal materials have not been observed nor reported as xenoliths from the studied area. Moreover, according to the Moho depth map of (Dehghani and Makris, 1984) the crustal thickness of the area ranges from 48 to 50 km.

The andesitic, dacitic and rhyodacitic of study area show high Na_2O/K_2O, high Sr, low Y, strongly high REE depletion and high LREE.

Several workers (Peacock et al., 1994; Sen and Dunn., 1994; Sen and Dunn., 1995) believe that such compositional characteristics of these rocks are consistent with their generation by melting of subducted oceanic lithosphere. The isotope values of initial $^{87}Sr/^{86}Sr$ (0.704273 to 0.705668) and εNd (+1.3 to +4.1) for these rocks as reported by Moradian (1997), indicates that pelagic sediment could not have been involved in the genesis of the andesitic and dacitic rocks. Partial melting of an eclogite source would generate melts that have high Sr/Y, high LREE, but low Y and low HREE (Defant and Drummond, 1990; Defant and Kepezhinskas, 2001; Martin, 1999; Martin et al, 2004). Controversy exists in the literature about the timing of the closure of Neo–Tethyan along the Zagros suture. Some authors infer a late cretaceous age for continental collision (Berberian and King., 1981; Alavi, 1994). A late Cretaceous age for continent–continent collision comes from the timing of the ophiolite emplacement, i.e. age of the youngest pelagic fossils involved in the Zagros ophiolites. However, this age has been shown to merely reflect the timing of ophiolite obduction due to collision of the passive margin of Zagros–Oman in an offshore intra–oceanic arc (Berberian, 1987), while a vast area of oceanic lithosphere still existed to the north of Zagros (Dercourt et al., 1986), yet to be subducted underneath central Iran during the Tertiary. An alternative idea is that continental collision along the Zagros suture occurred in the Miocene (Berberian et al., 1982; Sengör et al., 1988; Sengör et al., 1996).

Paleo–oceanographic constraints derived from carbon and oxygen isotopec data indicates that Neo–Tethys had a connection with the northern Indian Ocean until 14 Ma (Woodruff et al., 1995). This fact supports the Miocene reconstruction of Neo–Tethys by (Sengör et al., 1996) and is independent of regional geological evidence. Existence of widespread shallow marine and limited deep–marine Paleocene to Miocene sediments in the Zagros sub–zones are consistent with the south arm of the Tethys remaining open in to Miocene (Mohajjel et al., 2003). Opening of the Red Sea and the Gulf of Aden resulted in rotation of the Arabian plate with respect to Africa (Nubia and Somalia) since 30 Ma (Bonatti, 1987; Hempton, 1987; Guiraud and Boswoeth, 1999). This plate movement was responsible for oblique convergence between the Arabian plate and central Iran and final closure of Neo–Tethys.

Petrological studied carried out in this area and adjacent areas i.e. Mosahim, Madvar, Aj–Bala, and Aj–Pain indicates that post collisional magmas exhibit various

geochemical enrichment signatures. The significant character of post–collisional magmatism in this area indicates the progressive evolution of magmatic products from subalkaline to alkaline composition. A conspicuous characteristic of alkaline phase is the contemporaneous of mafic alkaline melts including melafoidites and alkali–basalts (Hassanzadeh, 1993). Onset of post–collisional magmatism in the late Pliocene to Pleistocene in this region with adakitic geochemical signatures, indicate the role of slab melting after cessation of subduction. The temporal and spatial relationship of the studied adakitic rocks may be attributed to slab roll–back and possibly break–off subducted Neo–Tethyan oceanic lithosphere beneath the Central Iranian continental microplate. Slab break–off may have led to thermal perturbation resulting in melting of detached slab and metasomatism of the mantle in Central Iran during the post–collisional event. Ascent of slab–derived magmas through thickened continental crust in this region could have been the cause of the observed crustal contamination resulting in high Rb/Sr ratios and increase of K_2O, Th and Y contents due to assimilation and fractional crystallization (AFC) processes. Evidence for AFC processes is marked by enrichment of K_2O over Na_2O and incompatible LILE enrichments such as Rb, Th and Ba relative to HFSE (Esperanca et al., 1992), (Fig. 12). The isotope values of initial $^{87}Sr/^{86}Sr$ (0.704 to 0.705) and εNd (+1.3 to +1.4) for this rocks respectively indicate AFC processes were involved in their formation (Moradian, 1997).

5– Conclusions

1– In the Sahand region (a part of volcanic belt of Iran) numerous subvolcanic dacitic to rhyodacitic domes were intruded in to different rocks during the Pliocene to Pleistocene. They exhibit porphyritic texture with phenocrysts of plagioclase, hornblende and minor biotite.

2– The geochemical characteristics of subalkaline dacitic to rhyodacitic rocks include high LILE, LREE, Sr, strongly fractionated REE patterns and low content of HREE and Y. The diagram of Y vs. Sr/Y and the diagram of $(La/Yb)_N$ vs. Yb_N show similarities with adakites.

3– The occurrence of adakitic among the post–collisional magmatic rocks could represent the first magmatic products after cessation of Neo–Tethys subduction in the volcanic belt of Iran.

4– The temporal and spatial adakitic rocks and alkaline volcanic rocks in the studied area can be attributed to slab break off and melting of detached slab and metasomatised mantle.

5– Volcanism along the dextral strike–slip faults is mainly related to extension, followed by strike–slip tectonics in the context of regional tension.

6– The variations in K_2O, LILE and HFSE contents in comparison with modern adakites can be attributed to fractionation and crystallization processes.

Acknowledgements

The authors would like to thank Prof. O. Karsli and Dr. M. Nasrabady for their kind and careful comments that made the manuscript improved.

References:

Alavi, M. 1994. Tectonics of the Zagros Orogenic belt of Iran: new data and interpretations. Tectonophysics: 220, 211– 238.

Alavi, M. 2004. Regional stratigraphy of the Zagros fold–thrust belt of Iran and

its proforeland evolution. American journal of Science: 304, 1–20.

Allen, M., Jackson, J., and Walker, R., 2004. Late Cenozoic reorganization of the Arabia–Eurasia collision and the comparison of short–term and long–term deformation rates. Tectonics: v. 23.

Ambraseys, N.N. and Melville C. 1982. A history of Persian earthquakes, Cambridge University Press.

Amidi, S.M., Emami, M.H., Michel, R. 1984. Alkaline character of Eocene volcanism in the middle part of Iran and its geodynamic situation. Geologische Rundschau: 73, 917–932.

Atherton, M. P., Petford, N. 1993. Generation of sodium–rich magmas from newly undererplated basaltic. Nature: 362, 144–146.

Behrouzi, A. Amini Fazl, A. Amini Azar, B. 1997. Geological Survey of Iran, 1:100,000 Series, Sheet 5265, Bostanabad.

Berberian, M. 1987. Oceanic evolution, rifting or drifting in the Red Sea. Nature: 330, 692–693.

Berberian, F., Berberian, M. 1981. Tectono–plutonic episodes in Iran. In Gupta, H. K., Delany, F. M. (Eds.), Zagros, Hindukosh, Himalaya. Geodynamic Evolution American Geophysical union, Washington, DC, pp. 5–32.

Berberian, M., King, G. C. 1981. Towards a paleogeography and tectonics evolution of Iran. Canadian Journal of Earth Sciences: 18, 210–265.

Berberian, F., Muir, I. D., Pankhurst, R. J., Berberian, M, 1982. Late Cretaceous and early Miocene Andean type plutonic activity in northern Makran and central Iran. Journal of Geological Society of London: 139, 605–614.

Bonatti, E. 1987. Oceanic evolution, rifting or drifting in the Red Sea? Nature: 330: 692–693.

Chung, S. L., Chu, M. F., Zhang, Y., Zie, Y., Lo, C. H., Lee, T. Y., Ching Ying Lan, C.Y., Xianhua Li, X., Zhang, O., Wang, Y. 2005. Tibetan tectonic evolution inferred from spatial and temporal variations in post–collisional magmatism. Earth Sciences Review: 68, 173–198.

Defant, J., and Drummond, S. 1990. Derivation of some modern arc magmas by melting of young subducted lithosphere, Nature: 374, 662–665.

Defant, M. J., Kepezhinskas, P. 2001. Evidence suggests slab melting in arc magmas. Eos, Transactions American Geophysical Union: 82. 67–69.

Dehghani, G. A., Makris, 1984. T. The gravity field and crustal structure of Iran. Neues Jahrbuch fur Geologie und Palaontologie–Abhandlungen: 168, 215–229.

Dercourt, J., Zonenenshain, L., Ricou, L. E., Kazmin, G., Lepichon, X., Knipper, A. L, Grandjacquet, C., Sbotshikov, I. M., Geyssant, J., Lepvrier, C., Pechersky, D. H., Boulin, J., Sibuet, J. C, Savostin, L. A., Sorokhtin, O., Westphal, M., Bazhenov, M. L., Lauer, J. P., and Biju– Duval, B. 1986. Geological evolution of the Tethys belt from the Atlantic to Pamirs since the Lias. Tectonophysics: 123, 241–315.

Derek, J., Thorkelson., Kartin, B. 2004. Partial melting of slab window margins: genesis of adakitic. Lithos: 79. 25–41.

Drummond, M. S., Defant, M. J. 1990. A model for trondhjemite–tonalite–dacite genesis and crustal growth via slab melting: Archaean to modern comparisons. Journal of Geophysical Research: 95, 21503–21521.

Esperanca, S., Crisci, M., de Rosa, R., Mazzuli, R. 1992. The role of the crust in the magmatic evolution of the island Lipari (Aeolian Islands. Italy). Contributions to Mineralogy and Petrology: 112, 450–462.

Farhoudi, G. H. 1978. A comparison of Zagros geology to island–arcs. Journal of Geology: 86, 323–334.

Forster, H., Fesefeldt, K., Kursten, M. 1972. Magmatic and orogenic evolution of the Central Iranian volcanic belt. In: 24th International Geology Congress, Section 2, pp. 198–210.

Ghasemi, A., Talbot, C. J. 2006. A new tectonic scenario for the Sanandaj–Sirjan Zone (Iran). Journal of Asian Earth Sciences: 26, 683–693.

Gill, J. B. 1981. Orogenic andesites and plate tectonics, Springer Verlag, Berlin. 390p.

Guiraud, R., Boswoeth, W. 1999. Phanerozoic geodynamic evolution of northeastern Africa and northwestern Arabian platform. Tectonophysics: 282, 39–82

Harker A., 1909. The natural history of igneous rocks, Macmillan, New York, 384pp.

Hassanzadeh, J. 1993. Metallogenic and tectonomagmatic events in the SE sector of the Cenozoic active continental margin of Iran (Shahre–Babak area, Kerman Province). Unpublished Ph. D thesis, University of California, Los Angeles, 204pp.

Hempton, M. R. 1987. Constraints on Arabian plate motion and extensional history of the Red Sea. Tectonic: 6, 687–705.

Irvine, T. N., Baragar, W. R. A. 1971. A guide to the chemical classification of the common volcanic rocks. Canadian Journal of Earth Sciences: 8, 523–548.

Jahangiri, A. 2007. Post–collisional Miocene adakitic volcanism in NW Iran: Geochemical and geodynamic implications. Journal of Asian Earth Sciences: 30, 433–447.

Jung, D., Kursten, M., Tarkian, M. 1976. Post–Mesozoic volcanism in Iran and its relation to the subduction of the Afro–Arabian under the Eurasian plate. In: Pilger, A., Rosler, A. (Eds.), A far Between Continental and Oceanic Rifting. Schweizerbartsche verlagbuchhandiung Stuttgart, pp. 175–181.

Kay, R. W. J. 1978. Aleutian magnesian andesites: melts from subducted pacific oceanic crust. Journal of Volcanology and Geothermal Research: 4, 117–132.

MacLean, W. H., Barrett, T. J. 1993. Lithochemical techniques using immobile elements. Journal of Geochemical Exploration: 48, 109–133.

Martin, H. 1993. The mechanism of petrogenesis of the Archean continental crust, comparison eith modern processes. Lithos: 30, 373–388.

Martin, H. 1999. The adakitic magmas: modern analogues of Archaean granitoids. Lithos: 46, 411–429.

Martin, H., Smithies, R. H., Rapp, R., Moyen, J. F., Champion, 2004. An overview of adakite–tonalite–trondhjemitegranodiorite (TTG), an Sanukitoid: relationships and some implications for crustal evolution, Lithos: 79, 1–24.

Maury, R. C., Sajona, F., Pubellier, M., Bellon, H., Defant, M.1996. Fusion de la croute oceanique dans las zones de subduction/collision recentes: l, example de Mindanao (Philippines). Bulletin de la Societe Geologique de France: 167, 579–595.

Mohajjel, M., Fergusson, C. L., Sahandi, M. R. 2003. Cretaceous–Tertiary convergence and continental collision, Sanandaj–Sirjan Zone ,western Iran. Journal of Asian Earth Sciences: 21, 397–412.

Moradian, A. 1997. Geochemistry, Geochronology and petrography of Feldspathoid Bearing Rocks in Urumieh– Dokhtar Volcanic Belt, Iran Unpublished Ph. D thesis, University of Wollongong, Australia, 412pp.

Peacock, S. M., Rushmer, T., Thompson, A. B. 1994. Partial melting of subducting oceanic crust. Earth and Planetary Science Letters: 121, 224–227.

Pearce, J. A., Parkinson, I. J. 1993. Trace element models for mantle melting: application to volcanic are petrogenesis. In: Prichard, H. M., Albaster, T., Harris, N. B. W., Neary, C. R. (Eds.), Magmatic Processes in Plate Tectonics, vol. 76. Geological Society of London Special Publication: pp. 373–403.

Pe–Piper, G., Piper, D. W. J. 1994. Miocene magnesian andesites and dacites, Evia, Greece: adakites associated with subducting slab detachment and extension. Lithos: 31, 125–140.

Pirmohammadi–Alishah, F. 2011. Petrology , Geochemistry and Petrogenesis of Volcanic Rocks in the East and Southeast of Sahand Volcano with Special Reference to the Pyroclastic Rocks, Ph. D thesis, University of Tabriz, Iran, 198pp.

Prouteau, G., Maury, R. C., Rangin, C., Suparka, E., Bellon, H., Pubellier, M., Cotton, J. 1996. Les adakites miocenes du NW Borneo, temoins de la fermenture de la proto–mer de Chine. C. R. Acad. Sci. Paris: 323 serie IIa, pp. 925–932.

Rapp, R. P., Shimizu, N., Norman, M. D., Applegate, G. S. 1999. Reaction between slab–derived melts and peridotite in the mantle wedge: experimental constraints at 3.8 GPa. Chemical Geology: 160, 335–356.

Rapp, R. P., Watson, E. B., Miller, C. F. 1991. Partial melting of amphibolite/eclogite and the origin of Archaean trondhjemites and tonalities. Precambrian Research: 51, 1–25.

Reagan, M. K., Gill, J. B. 1989. Coexisting calc–alkaline and high niobium basalts from Turrialba volcano, Costa Rica: implications for residual titanites in arc magma sources. Journal of Geophysical Research: 94, 4619–4633.

Ricou, L. E. 1994. Tethys reconstruction: plates, continental fragments and their boundaries since 260 Ma from Central America to South–eastern Asia. Geodinamica Acta: 7, 169–218.

Sajona, F. G., Bellon, H., Maury, R.C., Pubellier, M., Cotton, J., Rangin, C.

1994. Magmatic response to abrupt changes in tectonic setting: Pliocene–Quaternary calcalkaline lavas and Nb–enriched basalts of Leyte and Mindanao Philippines. Tectonophysics: 237, 47–72.

Sajona, F. G., Maury, R. C., Bellon, H., Cotton, J., Defant, M. J., Pubellier, M., Rangin, C. 1993. Initiation of subduction and the generation of slab melts in western and eastern Mindanao, Philippines. Geology: 21, 1007– 1010.

Sajona, F. G., Maury, R. C., Publlier, M., Letirrier, J., Bellon, H., Cotton, J. 2000. Magmatic source enrichment by slab–derived melts in a young post–collision setting, Central Mindanao (Philippines). Lithos: 54, 173–206.

Seghedi, I., Downes, H., Vaselli, O., Szakacs, A., Balogh, K., Pecskay, Z. 2004. Post–collisional Tertiary–Quternary mafic alkalic magmatism in the Carpathian–Pannonian region: a review. Lithos: 72, 117–146.

Seking, T.,Wyllie, P. J. 1982. Experimental simulation of mantle hybridization in subduction zones. Journal of Geology: 91, 511–528.

Sen, C., Dunn, T. 1994. Dehydration melting of a basaltic composition amphibolite at 1.5 and 2.0 GPa: implications for the origin of adakites. Contributions to Mineralogy and Petrology: 117,394–409.

Sen, C., Dunn, T. 1995. Experimental modal metasomatism of a spinel lherzolite and production of amphibole–bearing peridotite. Contributions to Mineralogy and Petrology: 119, 42–432.

Sengor, A. M. C., Altmer, D., Cin, A., Ustaomer, T., Hsu, K. J. 1988. Origin and assemble of the Tethyside orogenic collage at the expense of Gondwanaland. In: Audley– Charls, M. G., Hallam, A. (Eds.), Gondwana and Tethys. Geological Society of London, Special Publication: 37, 19–181.

Sengor, A. M. C., Natalin, B. A. 1996. Paleotectonic of Asia: fragments of a synthesis. In Yin, A., Harrison, T. M., (Eds.), The Tectonic Evolution of Asia Combridge University Press, Cambridge, 486–640.

Stocklin, J. 1974. Possible ancient continental margins in Iran. In: Burk, C. A., Drake, C. L., (Eds.), The Geology of Continental Margins. Springer, Berlin, 873–887.

Sun, S. S., and McDonough, W. F. 1989. Chemical and isotopic systematics of oceanic basalts: implications for mantle composition and processes. In: Saunders, A.D., and Norry, M.J., (Eds.), magmatism in ocean basins. Geological Society of Londen Special Publicatio: 42, 313–345.

Tatsumi, Y., Koyaguchi, T. 1989. An absarokite from a phlogopite–lherzolite source. Contrib. Mineral. Petrology: 102, 34–40.

Wilson, M. 1989. Igneous Petrogenesis: Global Tectonic Approach. Harper Collins Academic, 466p.

Winchester, J. A., Floyd, P. A. 1977. Geochemical discrimination of immobile elements. Chemical Geology: 20, 325–343.

Woodruff, F., Savin, S. M. 1989. Miocene deep water oceanography. Paleoceanography: 4, 87–140.